Chapter 7
Composite Fuselage Impact Testing and Simulation: A Model Calibration Exercise

Lucas G. Horta, Mercedes C. Reaves, Karen E. Jackson, Martin S. Annett, and Justin D. Littell

Abstract Results from a model calibration study of a composite fuselage front frame test article subjected to impact loading are presented. The effort, undertaken over a 2 year time period, involved both modal and impact testing of the front frame section of a composite fuselage test article. Data from both types of tests were used with multi-dimensional calibration metrics to assess model adequacy. Specifically, two metrics are used: (1) a metric to assess the probability of enveloping the measured displacement during impact, and (2) an orthogonality metric to assess model adequacy between test and analysis. Because the impact test is destructive, vibration test data were also collected for model assessments in terms of modes of vibration. To justify the use of vibration data for calibration of the impact model, the paper discusses how to assess the relevancy of vibration data for calibration of impact models. Finally, results from the impact test are discussed and compared to model predictions and model uncertainty bounds.

Keywords Model calibration • Uncertainty • Impact response • Composites

7.1 Introduction

Aircraft manufacturers continue to pursue lighter weight structures to make their vehicles more fuel efficient. Although composite materials have been studied for over 40 years, only a few manufacturers have truly moved forward with vehicles where a high percentage of the load bearing structure is made from carbon fiber composites. Aside from manufacturing hurdles that need to be overcome to make the designs affordable, predictability and crashworthiness are still two aspects of the design that need to be better understood. To shed some light on the challenges associated with modeling and validation of composite fuselages, the paper presents analysis and results from tests conducted using parts from a previously tested prototype composite fuselage section manufactured by Sikorsky Aircraft Corporation under the U.S. Army's Survivable Affordable Repairable Airframe Program (SARAP).

In this chapter, data from a vibration test and data from the impact test described in [1] are used to assess the adequacy of an LS-DYNA [2] model. Data from test and analyses are processed using multi-dimensional calibration metrics, initially presented in [3], that consider uncertainty and model adequacy from a multi-dimensional viewpoint. Impact data from simulations are used to determine the proper vibration test boundary conditions to recover key vibration modes. Orthogonality of impact and vibration shapes is used to determine which vibration modes are important during an impact test. Because not all vibration modes influence the impact behavior of the system, tests must be tailored to target specific vibration modes. Calibration results for the LS-DYNA model using both vibration and impact data are discussed. The paper organization is as follows: test article description, discussion of the calibration metrics, results from the application of the metrics to the test data, results from calibration efforts to reconcile the model for both vibration and impact tests, and concluding remarks.

L.G. Horta (✉) • M.C. Reaves • K.E. Jackson • M.S. Annett • J.D. Littell
NASA Langley Research Center, MS 230, Hampton, VA 23681, USA
e-mail: lucas.g.horta@nasa.gov; mercedes.c.reaves@nasa.gov; karen.e.jackson-1@nasa.gov; martin.s.annett@nasa.gov; justin.d.littell@nasa.gov

H.S. Atamturktur et al. (eds.), *Model Validation and Uncertainty Quantification, Volume 3: Proceedings of the 32nd IMAC, A Conference and Exposition on Structural Dynamics, 2014*, Conference Proceedings of the Society for Experimental Mechanics Series, DOI 10.1007/978-3-319-04552-8_7,

7.2 Composite Subfloor Test Article

To take advantage of sections of a composite helicopter fuselage previously tested by Sikosrky, the front frame section was removed from the fuselage and used in our study. Figure 7.1 shows a side view of the entire section as tested by Sikorsky that included the crew access opening with subfloor, front and rear bulkhead frames, and roof with overhead mass that represented the engine. Because parts of the fuselage section were damaged during a prior impact test, this study discusses results using only the front frame section of the fuselage, see Fig. 7.1.

An LS-DYNA simulation model, initially developed by Sikorsky, was revised and updated at NASA Langley. It now contains 37,111 nodes, 17,216 Belytschko-Tsay shell elements, 8,300 solid elements; and 2,200 concentrated masses. The model is depicted in Fig. 7.2. Results included in this chapter were obtained using the LS-DYNA Mat 58 material property card to represent the composite layups with Type 2 shell elements. Type 16 fully-integrated shells were used for vibration analysis only because Type 16 shells typically require up to four times the execution time of the Type 2 shells. Prior to switching the simulation to Type 2, simulation runs were completed to verify that the results did not change by using Type 2 shell elements. For Mat 58, some key material properties used in the simulation are listed in Table 7.1. The impact simulation lasted 20 ms, which required about 12 min of CPU to execute on a Windows-based computer with eight processors.

7.3 Time Domain Calibration

7.3.1 Metric 1: Displacement Norm

Calibration metrics quantitatively assess the accuracy of an analytical model. The metrics used in this work were initially discussed in [3] and are summarized here for completeness. To contrast these metrics with other approaches, the readers are referred to work by Oberkampf and Barone [4] and Schwer [5], which set forth scalar statistical metrics for use with time history data. Metrics in terms of mean, variance, and confidence intervals facilitate assessment of experimental data. For the current problem, instead of using response predictions at a particular point as a metric, a vector 2-norm (magnitude of vector) of the system response is used instead. An important benefit of using this metric is that it provides for a direct measure of multi-dimensional closeness of two models. In addition, when tracked as a function of time, closeness is quantified at each time step.

Model parameters not well known are assumed to be uncertain to evaluate the effect of parameter variations on the system response. By assuming that parameter values are uncertain, statistical measures of the metric can be computed and used to conduct model assessments. To facilitate the sampling process, parameter variations followed a uniform distribution

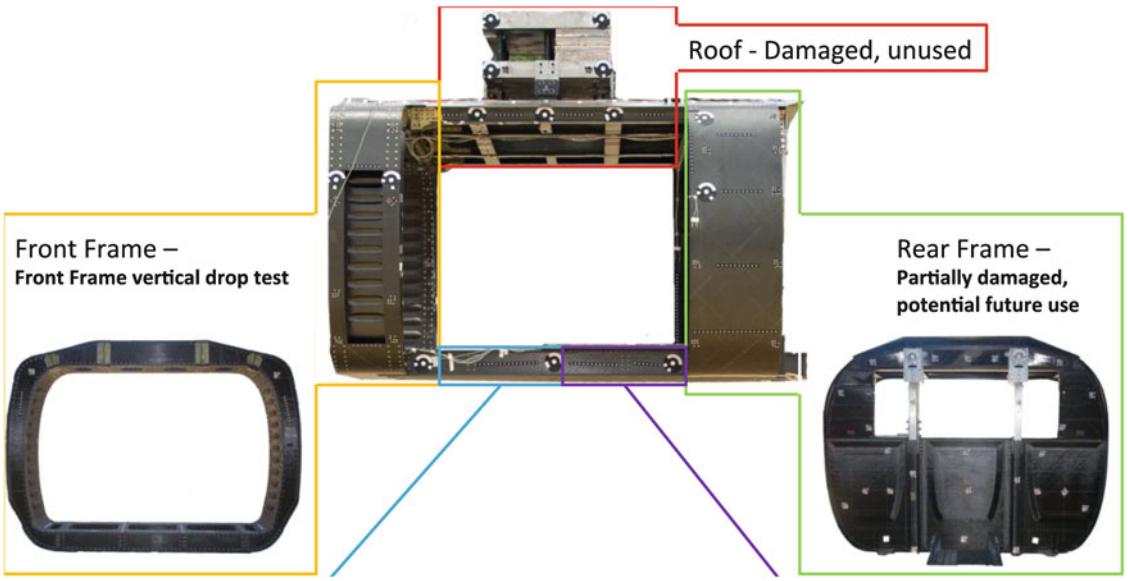

Fig. 7.1 Initial configuration of Sikorsky Composite Helicopter

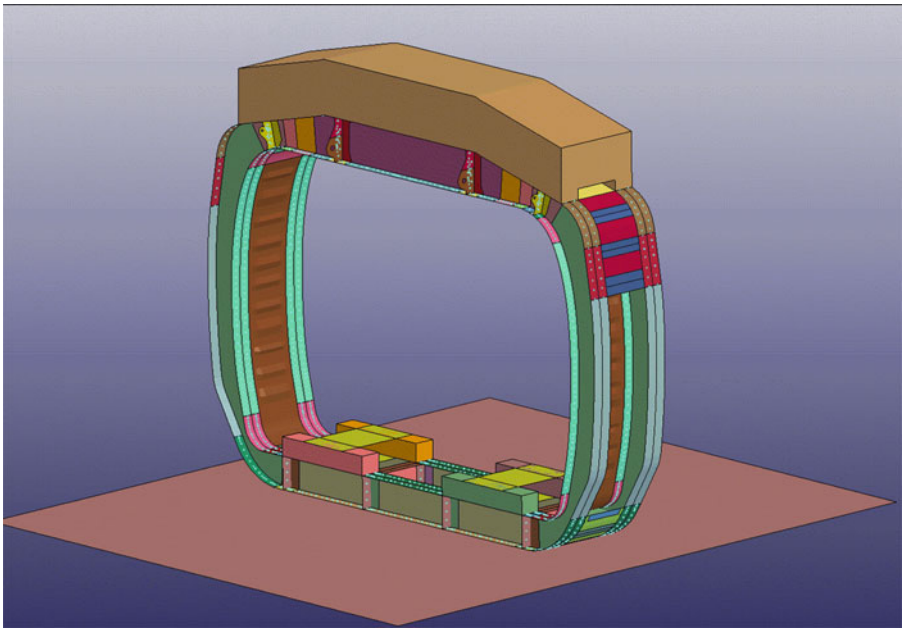

Fig. 7.2 LS-DYNA model of fuselage section

Table 7.1 Parameter uncertainty definitions

Parameter. No.	Properties	Nominal	Lower bound	Upper bound
1	Ea (lbs/in^2)	1.00E + 07	5.00E + 06	2.50E + 07
2	Eb (lbs/in^2)	1.00E + 07	3.00E + 05	2.50E + 07
3	GAB, GBC, GCA (lbs/in^2)	7.40E + 05	1.90E + 05	1.05E + 06
4	ERODS	0.15	0.02	0.60
5	θ_x roll (deg)	0.00	−0.50	0.00
6	θ_y pitch (deg)	0.00	0.00	0.50
7	Velocity (in/s)	−249.00	−255.00	−243.00

function. Statistical sampling is used to create a family of N equally probable parameter vectors with their corresponding responses, where N is user selected. For calibration it is important to estimate the probability of being able to reconcile test with predictions, assuming that both the model and parameter uncertainty are appropriate. To this end, let $Q(t,p) = \|v(t,p)\|_2$ be a scalar time varying function in which the response vector v is used to compute the 2-norm at time t as a function of the parameter vector p. Furthermore, let $\underline{\sigma} = min_{\forall p} Q(t, p)$ be the minimum value over all parameter variations, and let $\overline{\sigma} = min_{\forall p} Q(t, p)$ be the maximum value. Using these definitions and N LS-DYNA solutions corresponding to equally probable parameter vectors, a calibration metric is established to bound the probability of predicting different values of $Q(t,p)$ as:

$$M_1(t) = Prob(\underline{\sigma} < Q(t) < \overline{\sigma}) = \frac{N-1}{N} \tag{7.1}$$

This probability simply states that after N observations, the next observation has a probability better than $(N-1)/N$ of being within the computed bounds. Conversely, the probability that the model is capable of predicting experimental observations $Q_e(t)$ (in terms of 2-norm of responses) outside the analysis bounds is that less than $1/N$. Note that N controls the tightness of the bounds and also the number of LS-DYNA solutions required.

7.3.2 Metric 2: Orthogonality

Data from either test or analysis are often collected at fixed time intervals from multiple sensors. It is convenient to assess the validity of models using time invariant quantities. For example, in traditional vibration analysis, structures are tested and models are verified using vibration modes and frequencies. Analogously, impact data can also be assessed using time

invariant quantities, which will be referred to as impact shapes and impact shape contributions. The process of computing these time invariant quantities uses singular value analysis. Given n samples of the response sampled at ΔT, time history data can be decomposed as:

$$\begin{Bmatrix} Y \\ Y_e \end{Bmatrix} = \begin{bmatrix} y(0) & y(\Delta T) & \dots & y(n\Delta T) \\ y_e(0) & y_e(\Delta T) & \dots & y_e(n\Delta T) \end{bmatrix} = \begin{bmatrix} \Phi \\ \Psi \end{bmatrix} \sum G \tag{7.2}$$

The rightmost equality in (7.2) uses singular value decomposition (SVD) of the time history data. Data are divided into m measurements stored in Y, and q unmeasured values stored in Y_e. In this decomposition, the basis matrices $\Phi \in \mathbb{R}^{mxh}$ and $\Psi \in \mathbb{R}^{qxh}$, referred to as basis or impact shapes, contains the time independent spatial distribution of sensors, whereas $G \in \mathbb{R}^{hxn}$ contains time variations, and $\sum$ contains the non-zero singular values $\{\sigma_1\ \sigma_2\ \cdots\ \sigma_n\}$. Individual impact shape contributions are calculated as:

$$\delta_i = \frac{\sigma_i}{\sum_{i=1}^{n} \sigma_i} \tag{7.3}$$

By construction, the sum of the impact shape contributions equals one. With this decomposition approach, a multi-dimensional metric is easily established. Specifically, the impact shape matrix computed with (7.2) from analysis and test are compared using orthogonality. Numerically, the orthogonality metric is computed as:

$$M_2 = \widehat{\Phi}\widehat{\Gamma} \tag{7.4}$$

Where $\widehat{\Phi}$ is sized $m \times h$ with h measured impact shapes at m locations and $\widehat{\Psi}$ sized $m \times h$, are shapes computed using simulation data. Both $\widehat{\Phi}$ and $\widehat{\Psi}$ have been normalized such that $\widehat{\Phi}^T\widehat{\Phi} = I$ and $\widehat{\Psi}^T\widehat{\Psi} = I$. Because individual impact shape vectors are stacked column-wise, the orthogonality metric M_2 is sized $h \times h$ with diagonal values corresponding to the vector projection numerical value. If vectors are identical then their projection equals 1. Consequently, multi-dimensional closeness is judged based on similarity of impact shapes and shape contributions.

7.4 Pretest Analysis for Modal Test

Traditional vibration tests are often guided by control requirements or the need to verify structural models for load assessments. Those requirements provide test engineers with specific vibration modes to target during tests. Unfortunately, vibration data are rarely used in the calibration of models to predict impact responses. However, if tailored properly, vibration tests can provide relevant data about the linear behavior of the models prior to impact. Tailoring of the vibration test requires the proper boundary conditions for vibration analysis. Techniques to identify which vibration modes to target have not been clearly stated in the open literature. In this work, orthogonality of impact shapes and vibration modes will establish which vibration modes to target during vibration testing. Impact shapes are computed by post-processing of time histories from a nonlinear simulation (see (7.2)), whereas vibration shapes are computed from an eigenvalue solution using the system mass and stiffness matrices. Several different boundary conditions for vibration testing were examined, and it was determined that simply supporting the fuselage under the floor while mass loading the top provided the best test configuration from an orthogonality viewpoint. Figure 7.3 shows pre-test orthogonality results between vibration modes and impact shapes. Numerical values near 1.0, indicated with dark colors, correspond to nearly identical shapes. From these results, vibration modes at 73 and 144 Hz are the only two vibration modes that needed to be targeted in the modal test. These two vibration modes are similar to two impact shapes that contribute 73 % of the impact response.

7.4.1 Modal Testing

Modal testing of the fuselage section concentrated on extracting the two critical modes identified in the pre-test analysis. In the modal test configuration, the test article weighed 1,610 lb, including 368 lb for the fuselage section, 423.5 lb for the floor ballast, and 818.5 lb for the upper ballast. A montage of pictures from the modal test is shown in Fig. 7.4. A front-left view of the entire fuselage test section is shown in the center of Fig. 7.4. Close-up photographs of the left, right, top, and floor

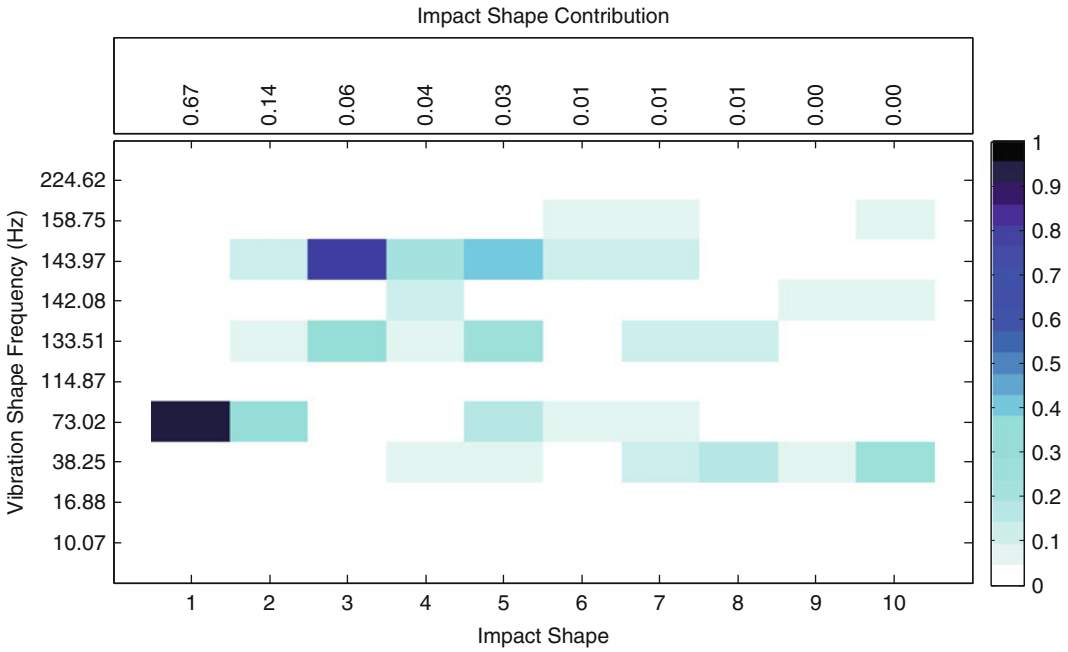

Fig. 7.3 Orthogonality of vibration modes and impact shapes

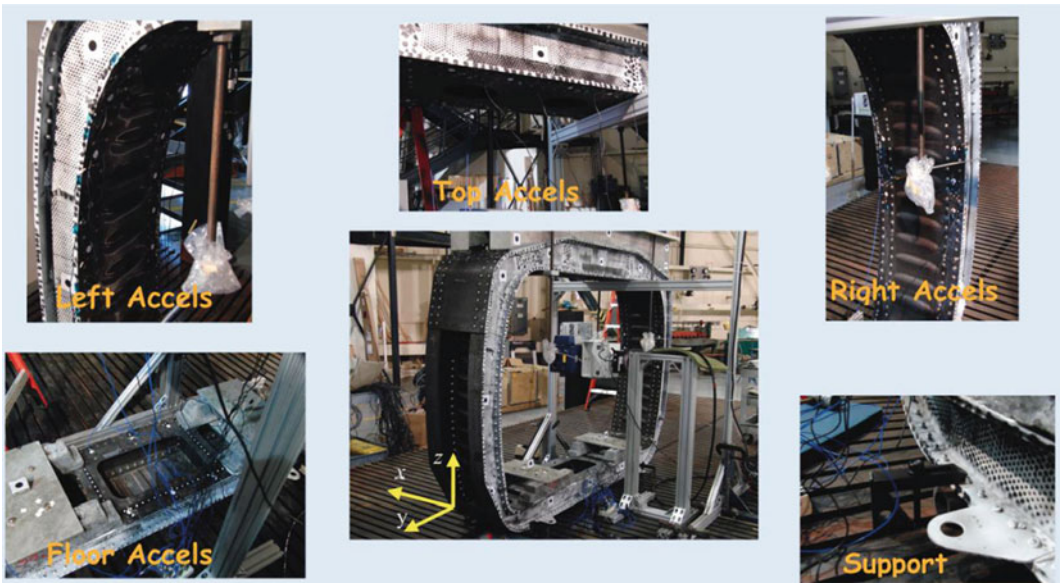

Fig. 7.4 Montage of composite fuselage test section undergoing modal testing

accelerometers are shown including a view of the bottom clamp support. For testing, the fuselage rested on a 3-in. diameter tube placed on metal plates on the laboratory floor and clamps kept the fuselage from lifting off the floor. For all testing PCB Piezotronics accelerometers were used with nominal sensitivity of 500 mV/g. For excitation, a PCB Piezotronics impact hammer with a hard tip was used with an in-line load cell to measure the input force. Because only nine accelerometers were available, testing was conducted by sections (i.e. left, top, etc.). For each data set, the fuselage was hit with the impact hammer in all three directions. Although most of the accelerometers were placed to measure accelerations normal to the inner surface of the fuselage, two accelerometers were placed to measure the out-of-plane accelerations (i.e. x-direction). Acceleration data were collected from 0 to 256 Hz with a frequency resolution of 0.5 Hz. A total of 34 acceleration measurements were collected. From the pre-test analysis, only two vibration modes were deemed important for impact: the fourth vibration mode at 73 Hz and the eighth mode at 144 Hz. The mode at 144 Hz is primarily the fuselage floor moving in the vertical direction, and the mode at 73 Hz involves motion of the entire cross section.

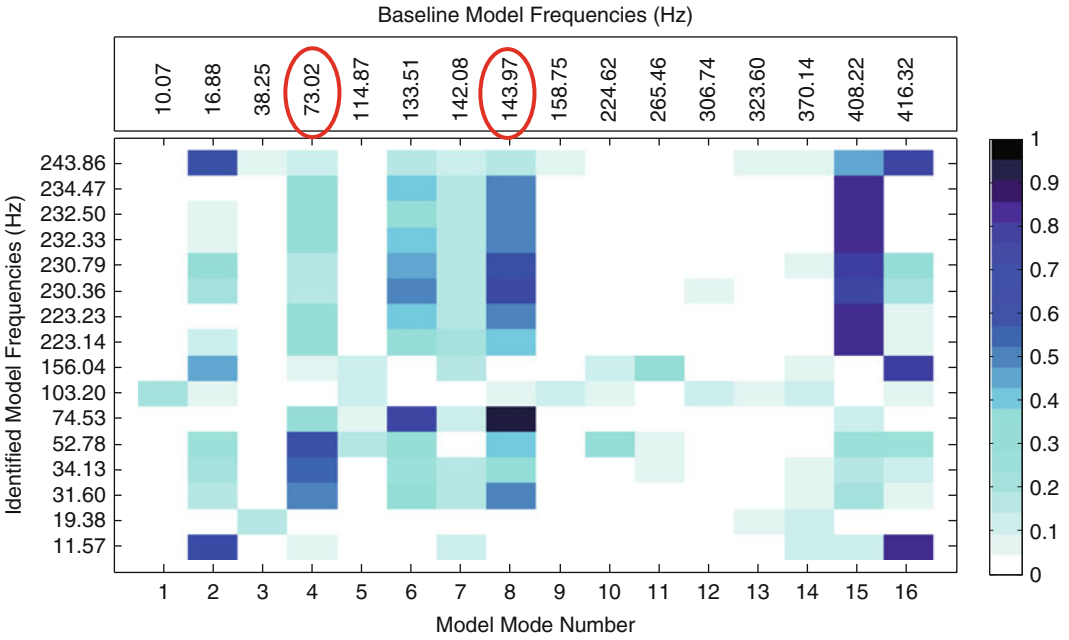

Fig. 7.5 Orthogonality of test versus LS-DYNA predicted modes

Frequency response functions from the vibration tests with 34 accelerometers were analyzed using the MATLAB SOCIT (System Observer Controller Identification Toolbox) [6] and the Frequency Domain Identification Toolbox [7]. Frequency data were analyzed to determine the experimental mode shapes and frequencies used to compare with analysis. The results of this analysis are reported next.

7.4.2 Comparison of Modal Test Results with Analysis

Figure 7.5 shows orthogonality values between the identified vibration mode shapes and the LS-DYNA predicted mode shapes. Readers should note that although orthogonality is used again, in this case the comparisons use vibration modes instead of impact shapes, as described earlier. Figure 7.5 also lists the frequencies of the identified modes and the predicted frequencies from LS-DYNA. Circled in red are the two target modes based on pre-test predictions. All orthogonality results are weighted using the reduced mass matrix M such that the orthogonality matrix is computed as $0 = \Phi_d^T M \Phi_t$, where Φ_d are the mode shapes from an implicit solution from LS-DYNA and Φ_t are the mode shapes from the modal test. Pairing of test and analysis modes was based on orthogonality values (e.g. modes with orthogonality values near 1.0 have similar shapes). In some cases, one analysis mode matched several experimental modes, which is probably caused by an insufficient number of sensors. For our purposes, if an analysis mode appears to be similar to an identified mode(s) (i.e. high orthogonality value), then it is assumed that the mode exists but was not well identified.

As shown in Fig. 7.5, the first analysis target mode at 73 Hz appears to be similar (i.e. high orthogonality value) to identified modes at 53, 34, and 32 Hz. Furthermore, the LS-DYNA predicted mode at 408 Hz appears to be similar to identified modes in the 230–234 Hz range. Similarly, the second target mode at 144 Hz appears to be similar to an identified mode at 74.5 Hz. Based on these results, it should be apparent that the LS-DYNA model is consistently over-predicting the frequencies of the fuselage vibration modes and therefore changes to the model should seek to reduce all predicted frequencies.

Post-test examination of the baseline model revealed that frequency results were very sensitive to the boundary condition. In particular, the simply supported boundary condition, which was initially represented as a pin condition along the line of nodes in contact with a tube placed under the fuselage, had to be modified so translations were only constrained at four points. After revising the boundary condition the LS-DYNA model produced the results shown in Fig. 7.6. The two model critical frequencies have now dropped to 62 and 105 Hz.

Animations of these two critical modes showed that motion occurred primarily on the floor. Although the pre-test analysis showed that exciting the fuselage at the top was adequate, during testing it was difficult to get enough energy into these

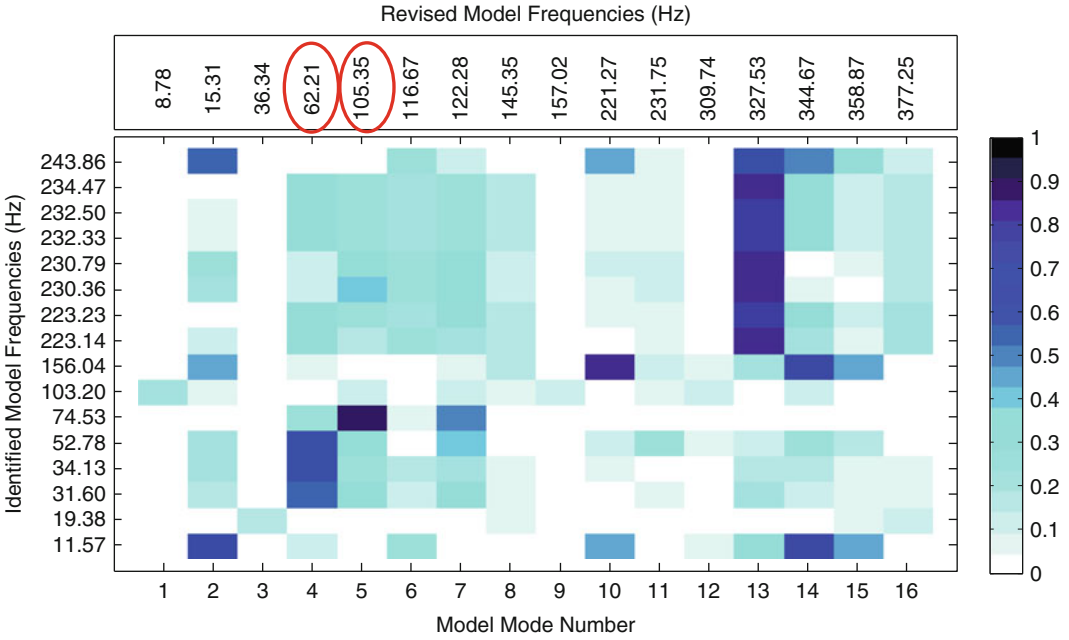

Fig. 7.6 Orthogonality results for revised LS-DYNA model and test

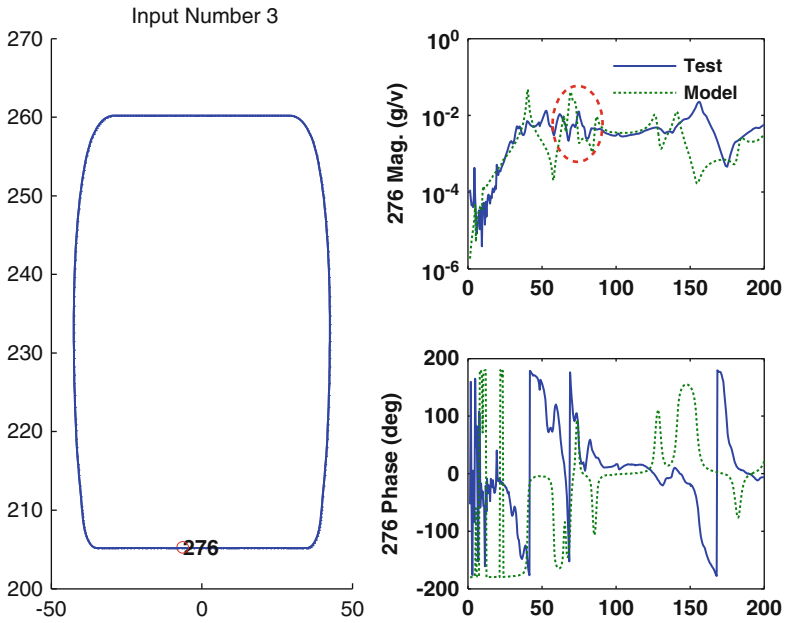

Fig. 7.7 *Left* plot shows a front view of the inner surface of the fuselage with floor node 276 marked and on the *right* is the corresponding frequency response comparison

modes. Figure 7.7 shows a front view of the fuselage inner surface with the location of floor node 276 marked and the corresponding analytical and test frequency response functions. Note that in the critical range (circled in red) the target modes are not clearly excited and therefore are difficult to identify.

As an example of needed corrections, the second target mode, which had the highest orthogonality value, was used as a reference to estimate changes required to get the frequencies to agree. Specifically, to get a frequency reduction from 105.4 to 74.5 Hz one would need to reduce the modulus to about 71 % of its original value. In fact, to test this assumption, the Mat 58 unidirectional tape and fabric material properties EA, EB, GAB, GBC, and GCA were all adjusted using optimization to minimize the error between test and analysis. Although a modulus reduction as initially suggested will greatly improve frequency agreement for the target modes, other non-critical modes were adversely affected.

7.5 Impact Testing

Impact testing of the fuselage section took place at the vertical drop tower in the LandIR facility at NASA Langley. An overhead portal frame on the drop tower was used to attach the fuselage section as shown in Fig. 7.8. For testing, the portal frame with the test article was raised to a height of 91 in. and dropped to achieve a nominal 21 ft/s (252 in/s) velocity. Prior to test, the system weighted 5,884 lbs, which included the portal frame, the upper ballast mass, lower floor ballast mass, and the test article. Photogrammetry (PG) data were acquired from both sides of the test article but only data from the south facing cameras sampled at 10 kHz will be presented. These south facing cameras were used to measure the impact conditions, time histories of the displacement, and velocity for 16 discrete targets.

Post-test processing of the PG data revealed that the velocity at impact was 20.75 ft/s (249 in/s) and the total vertical crush of the test article was 7.25 in. In addition, the fuselage section was found to have a pitch angle at impact of 0.42° and a roll angle of 0.29°. For reference, pitch rotates the top of fuselage in the photograph of Fig. 7.8 towards the back whereas roll simply rotates the entire section. Shearing and brittle fracturing failures occurred at the sides near the lower corners of floor. Delamination of side panels occurred near the crush front on the lower sides.

Four still images extracted from the high-speed videos are shown in Fig. 7.8. The first image in the upper left shows the test article immediately before impact. The upper right image shows the specimen 10 ms after impact. At this time, the bottom of the test article has contacted the ground and the sides have bowed out. Localized failure due to shear and buckling of the individual layers has begun; however, the test article largely retained its structural integrity. The lower left picture shows the test article 25 ms after impact. At this point in time, large-scale failures due to shearing and brittle fracturing in the floor structure were present in the lower corners. The lower right image shows the test article 50-ms after impact. The floor structure has completely separated from the rest of the test article.

Fig. 7.8 Image sequence of the fuselage section drop test from the southeast camera

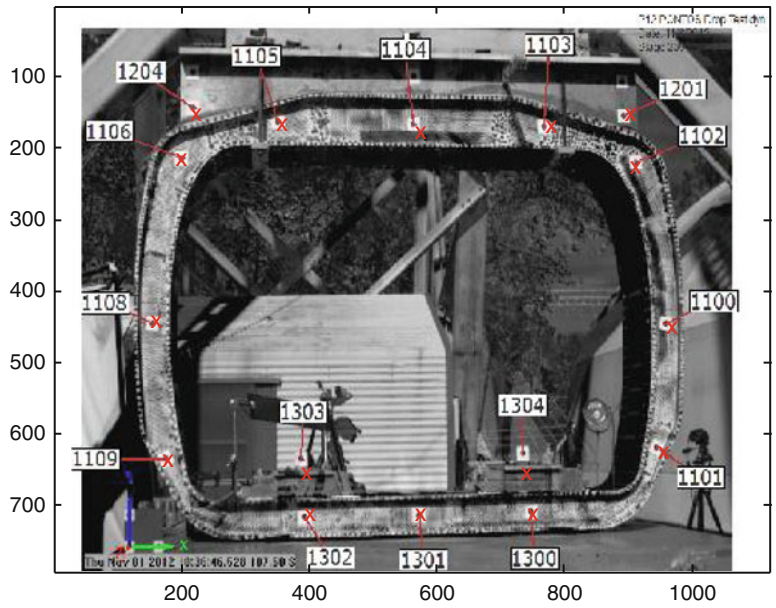

Fig. 7.9 South facing camera image with LS-DYNA nodes superimposed (*red* x)

7.5.1 Photogrammetry Data Processing

Data collected from the south facing cameras at 10,000 frames per second were processed and converted to time histories for each target. Before using the target time histories they needed to be processed to map targets to LS-DYNA nodes. Only PG data from the first 20 ms were used which corresponded to times when the floor was still attached. Figure 7.9 shows a south-view photograph of the fuselage with the 16 PG targets mapped to the closest LS-DYNA nodes, which are marked with red x's. Targets were matched to LS-DYNA nodes if they were within 2 in.

7.6 Multi-dimensional Model Calibration

After processing of the PG data, the next step in the model calibration process is to assess the model adequacy. If the established metrics are met, then models can be accepted. Models are seldom found to be adequate without the need for adjustments. In the current approach certain parameters are assumed to be uncertain and their values are varied to evaluate the probability of being able to reconcile test with analysis. Instead of looking at individual target displacements, the process used displacement bounds as a metric to assess the ability to reconcile the model. Specifically, the reconciliation distance between the model and test is measured using a vector 2-norm. With the south view displacement data, the response vector contained 48 entries corresponding to x, y, and z displacements for 16 targets. At each time step, differences between PG and LS-DYNA are compared in terms of a vector 2-norm, i.e. distance. Using norms, the worst error is always tracked and model revisions are focused on correcting those trouble areas.

To assess variations in response predictions, analyses were conducted assuming that the parameter set shown in Table 7.1 were not well known. Specifically, parameters were assumed to be uniformly distributed within the bounds defined in Table 7.1. A random sampling of these parameters was used to execute 100 LS-DYNA runs. For each LS-DYNA run, the displacement magnitude norm was computed at all 16 targets. Figure 7.10 shows the norm of displacement upper and lower bounds from 100 LS-DYNA runs (dashed blue) plotted along with the displacement norm computed with PG data (solid red). Reconciliation of the model with test is not possible for the first 9 ms because the analysis consistently over-predicted the response in all 100 LS-DYNA runs. In fact, using the worst case norm values the displacement error cannot be made less than 0.4 in., within the first 9 ms. At later times, there is enough freedom in the parameter selection to reduce the displacement error. Unfortunately, at this point, an uncertainty model for the parameters has not been found to fully encompass the test results.

Orthogonality results of the measured versus predicted impact shapes are compared using the south PG data. Figure 7.11 shows the first five impact shapes computed using PG data and those corresponding to the analysis when using the baseline parameters. The ordinate shows the fractional shape contributions for analysis whereas test results are shown across the top.

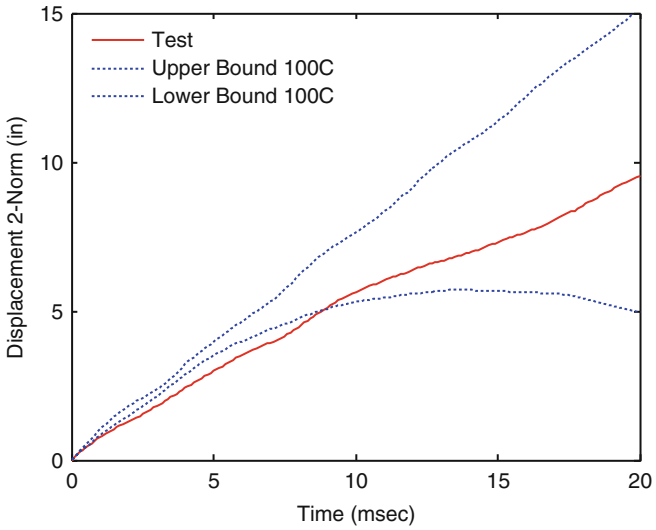

Fig. 7.10 Predicted uncertainty displacement bounds (*dashed-blue*) versus test (*solid-red*) for 48 targets using 100 LS-DYNA runs

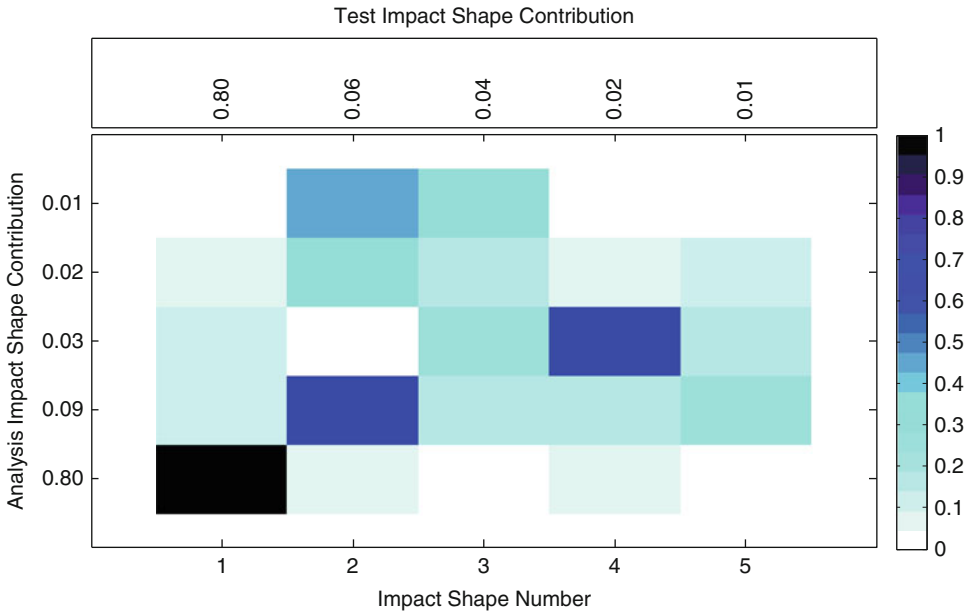

Fig. 7.11 Orthogonality of test impact shapes versus analysis

Note that the first impact shape from test and analysis have an orthogonality value near 1. Furthermore, the first measured impact shape is responsible for 80 % of the measured response which agrees with analysis predictions. On the other hand, the second test impact shape contributes 6 % of the response as compared to the 9 % predicted by the analysis. For good time response agreement (at all sensor locations) it is important than both the shapes and contributions be in agreement between test and analysis. To give the readers a sense of the deformation pattern corresponding to the main impact shapes, Fig. 7.12 shows side-by-side comparisons of test (top) and analysis (bottom) at the measured locations for the first two impact shapes. The impact shape outline is constructed by connecting all the target deformations shown in the photograph of Fig. 7.9. Clearly both impact shapes displayed show significant floor motion, which is consistent with test observations.

Finally sensitivity results are shown in Fig. 7.13 when using the 7 parameters defined in Table 7.1. With these 7 parameters, a variance-based sensitivity estimate was computed using the 100 LS-DYNA runs to create a surrogate model which was then used to compute 5,000 estimates of the 16 target responses. Contributions from each parameter to the total variance are color coded with the sum total contribution ≤ 1. These sensitivity results are used to assess the importance of the various parameters in all areas but in particular in areas where the model responses do not agree with test. From the sensitivity results, it is clear that the first 9 ms of the response is dominated by the roll angle θ_x variations and the impact velocity. Hence to affect the first 9 ms one would need to change the roll angle and velocity beyond the values listed in Table 7.1, which is not justifiable. More importantly, a surprising finding is that at later times the non-physical parameter ERODS controls the system response. ERODS is a failure parameter that when set to 1 tells the program to remove elements with 100 % straining.

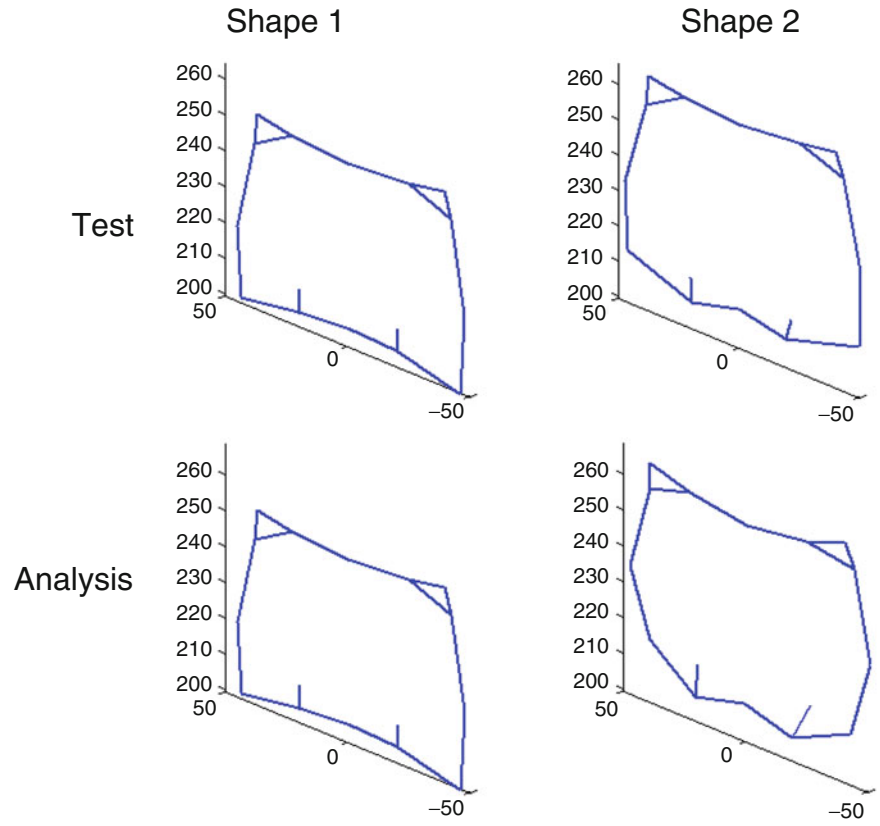

Fig. 7.12 Qualitative comparison of the first two measured and predicted impact shapes; first column shape 1 and second column is shape 2

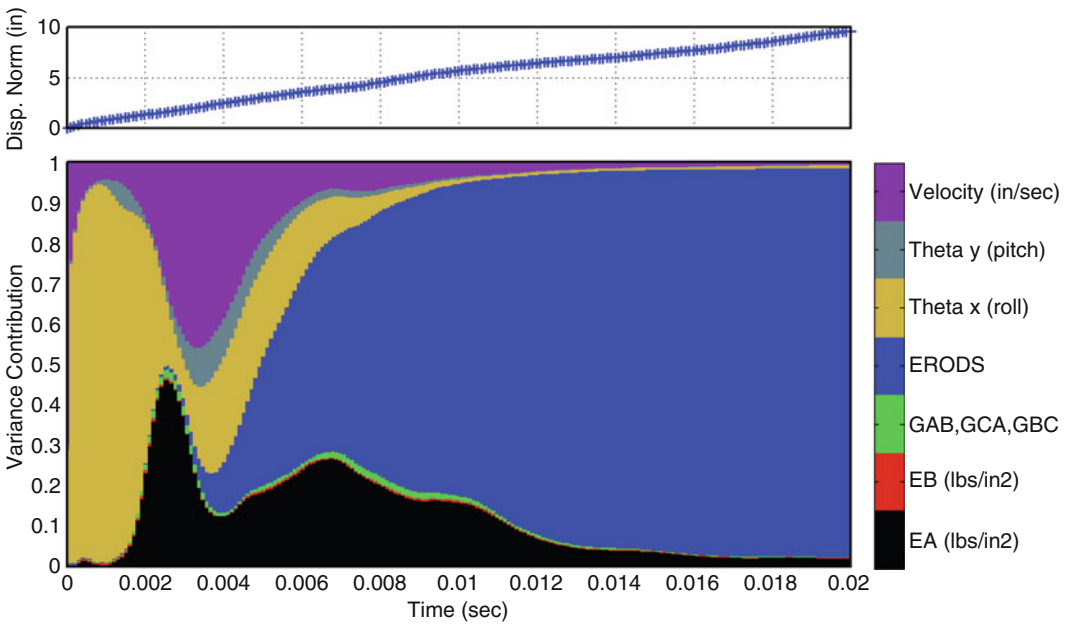

Fig. 7.13 Sensitivity results for fuselage model

Unfortunately, it is very difficult to set ERODS values based on component test data. An optimization search for a parameter set to minimize the error between displacement test and analysis was unable to reduce the displacement norm error to less than 1.22 in. For most parameter values the error was well within $1.22/\sqrt{3}$ inches in any particular direction.

Overall, in order to reconcile the analysis with test results one needs to consider both tests: vibration and impact. Recall that the vibration test results suggested that the modulus of the material needed to be reduced to 71 % of their original values

while the impact response suggest a need to increase the modulus. Although this finding seems paradoxical, it only points out the importance of using multiple tests and different types of tests for calibration of models. In fact, a static test would have helped tremendously in solving this dilemma.

7.7 Concluding Remarks

The paper discussed results from modal and impact tests along with the corresponding analysis of a composite fuselage section fabricated by the Sikorsky Aircraft Corporation under the US Army's SARAP. Two model calibration metrics were used throughout the paper to evaluate the model adequacy. Metric 1 measured the proximity of the model response to test, which, when used in conjunction with statistical sampling, allows users to construct analytical bounds of the response of interest. In contrast, Metric 2 compared the basis vectors or impact shapes that made up the response from test and analysis. This approach is analogous to comparing vibration modes in a modal test. In fact, the connection between vibration and impact shapes was established and used for pre-test vibration analysis. In the end, target modes recovered from the vibration test suggested that the overall stiffness of the model needed to be reduced.

Photogrammetry data from 16 targets (3 directions per target) was used to compute calibration metrics and to assess model adequacy post-test. Using the metrics and the parameter uncertainty representation, the model is irreconcilable with test. However, achievable levels of agreement in terms of displacements were established. More importantly, data from two distinct tests –a modal test and an impact test– suggested drastically different changes in the model parameters. Specifically, the vibration data suggested that the overall modulus needed to be reduced while the impact data suggested that the modulus should have been increased.

References

1. Jackson KE, Littell JD, Horta LG, Annett MS, Fasanella EL, Seal MD (2013) Impact testing and simulation of composite airframe structures. To appear as NASA TM
2. Hallquist JQ (2010) LS-DYNA keyword user's manual. Version 971, Revision 5.0, Livermore Software Technology Company, Livermore, CA, May 2010
3. Horta LG, Reaves MC, Annett MS, Jackson KE (2011) Multi-dimensional calibration of impact models. Chapter 15. In: Aeronautics and astronautics. Edited by Max Mulder, Published by Intech, Croatia. ISBN 978-953-307-473-3. 307- 473-3, pp. 441–457
4. Oberkampf WL, Barone MF (2006) Measures of agreement between computation and experiment. Validation metrics. Journal of Computational Physics 217:5–56
5. Schwer LE (2007) Validation metrics for response histories: perspectives and case studies. Engineering with Computers 23(4):295–309
6. Juang J-N, Horta LG, Phan M (1992) System/observer/controller identification toolbox. NASA TM 107566, February 1992
7. Horta LG, Juang J-N, Chen C-W (1996) Frequency domain identification toolbox. NASA TM 109039, September 1996